Calcium phosphate powder synthesis by out-of-phase pulsed sonoelectrochemistry

A.L. Daltin, S.. Beaufils, T. Rouillon, P. Millet, J.P. Chopart

Calcium phosphate powder synthesis by out-of-phase pulsed sonoelectrochemistry

A.L. Daltin[a*], S. Beaufils[a,b], T. Rouillon[b,c], P. Millet[a,d], J.P. Chopart[a]

[a]*Laboratoire d'Ingénierie et Sciences des Matériaux (LISM), EA 4695, URCA, B.P. 1039, 51687 Reims Cedex 02, France*
[b]*Inserm, UMR 1229, RMeS, Regenerative Medicine and Skeleton, Université de Nantes, ONIRIS, Nantes, F-44042, France*
[c]*Université de Nantes, UFR Odontologie, Nantes, F-44042, France*
[d]*Centre Hospitalo-Universitaire de Reims, 51100 Reims, France*

ARTICLE INFO

Keywords:
Ultrasound
Nanopowder
Calcium phosphate
Sonoelectrochemistry
Electrodeposition
Nanorod

ABSTRACT

High aspect ratio calcium phosphate (CaP) nanorods were achieved by out-of-phase pulsed sonoelectrodeposition from electrolytic aqueous bath composed of calcium nitrate, ammonium dihydrogenophosphate and surfactant at pH of 4.9. The nature of CaP phases was determined by powder X-ray diffraction (PXRD), Fourier Transform InfraRed spectroscopy (FTIR) and energy dispersive X-ray spectroscopy (EDX). The results reveal the predominantly presence of calcium deficient hydroxyapatite (CDHA). The transmission electron microscopy (TEM) analyzes highlighted that the nanorods are polycristalline and have an aspect ratio up to 30.

1. Introduction

Due to interest in biomedicine, current work focuses on shape and high aspect ratio of calcium phosphate (CaP) nanoparticles [1]. This kind of particles are needed for numerous applications such as bone tissue engineering, applications as nanoprobes, nanosensors, in the biosensing of pathogens or proteins, biofluoresent labeling, DNA probes, separation and purification of biological molecules and cells. Controlled CaP nanoparticles shapes and sizes are critical in improving the biocompatibility, bioactivity and osteoconductivity properties while avoiding cytotoxicity for materials used in biomedical applications [2-5]. Moreover, CaP materials can be used as chemical engineering materials such adsorbents, catalysts and catalysis supports or mechanical reinforcements. Shape is just as important as the size of these particles [6]. The interactions between CaP nanoparticles shape/size and their performances require a better control of their design and are the subject of many researches as those for hydroxyapatite fibers (HAF) [7]. There is a great variety of methods for the preparation of CaP nanoparticles, but very few of them are satisfactory in terms of economics mainly due to the diverse materials needed in the synthesis and the complex and expensive processes. Their performances can be reduced due to wide particle size distribution and the presence of phase impurities which usually occurs in the crystal structure. CaP synthesis can also be obtained by low or high temperature method. Low temperature methods can be divided into 2 categories: dry and wet. The dry methods, solid state and mechanochemical, give particle size distribution usually wide, while some wet methods could give nanosized particles with narrow particle size distribution. That is what sonochemical method allows where the chemical precipitation method induces variable particle size distribution [8-9]. The electrodeposition of CaP nanoparticles has progressed significantly since the 2000s as shown in fig. 1. Numerous types of materials have been synthesized coupling ultrasound to electrodeposition methods [10], but to this day no work has been published on an out-of-phase pulsed sonoelectrochemical synthesis, even if particles could be obtained by sonoelectrochemical or pulsed sonoelectrochemical methods as for CaP coatings deposited on carbon cloth electrodes [11].

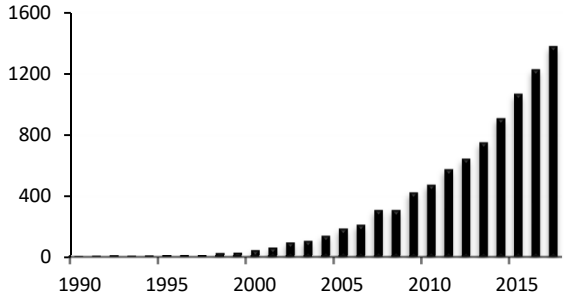

Fig. 1 CaP nanoparticles electrodeposition papers (from Google Scholar)

* *Corresponding author.*
E-mail address: al.daltin@univ-reims.fr (A.L. Daltin)

The specificity of out of phase pulse sonoelectrodeposition is the dual role of ultrasonic horn as working electrode and ultrasound emitter working in pulse mode. Among the various types of sonoelectrochemistry cells, the sonoreactor where the ultrasound horn is converted into working electrode was first introduced by Reisse, Deplancke and Winand for electrodeposition of copper and electroreduction of benzaldehydes and benzoquinone [12]. Out-of-phase pulse sonoelectrodeposition allowed the synthesis of various materials including pure metals such as Cu [13] Au [14], Mg [15], Pt [16]; Metallic alloys: Fe75Co25 [17], Co65Fe35 [18], Fe-Cr [19], Co-Pt in C cages [20], Fe-Pt [21], Fe-Pd [22] ; Metal oxide semiconductors: Cu_2O [23], CdSe [24] ; Conductive polymers : PANI [25] and core shell: Cu@Ag [26], Cu-Pt@Pt [27]. This technique has shown its ability to generate controlled nanoscale particles with a narrow size distribution. However, before the present study no inorganic material, excluding oxides, was synthesized by this method. Given the interest in nanoparticles of calcium phosphate and the many potential applications, we found it was important to initiate the study of their synthesis by this method to better control their morphology at a nanoscale. This practical combination may develop simple and cost-effective innovative approach to prepare well crystallized and narrow grain size distribution CaP nanoparticles. This process, which involves the production of an ultrafine material layer on the surface of the titanium sonotrode (working electrode) during a time pulse current or potential (t_{ON}) allows the synthesis of size-controlled nanoparticles, with very narrow size distribution and high specific surface area [23]. The short electrochemical pulse is immediately followed by a short pulse of high intensity ultrasound (t_{US}) that removes the particles from the cathode surface and replenishes the double layer with cations by stirring the solution. Then a rest time (t_{OFF}), without current or ultrasonic vibrations, follows the two previous pulses and it is useful to restore the initial conditions close to the sonoelectrode surface.

The goal of this work is to synthesize CaP NPs with high aspect ratios. That should for example enhance the adhesion and proliferation of osteoblasts, increase osteoblastic functions [28-29] resulting in higher osteoconductivity, bioactivity and osteoinductivity than conventional particles and microphases ceramics and enhance composites 'properties and mechanical strengthening [30-31]. For this purpose, a composition close to that of hydroxyapatite (HA) or calcium deficient hydroxyapatite (CDHA) is expected [32]. Here the challenge is to prepare controlled nanoscale CaP particles with a narrow size distribution and high aspect ratio particles without template, which would allow a production of larger batch size.

2. Experimental

2.1. Materials

CaP nanoparticles have been synthesized from electrolytic aqueous bath composed of 0.042 M calcium nitrate $Ca(NO_3)_2$, $4H_2O$, 0.025 M ammonium dihydrogen phosphate $NH_4(H_2PO_4)$, 99% purity and sodium hydroxide (NaOH), purity 98% purchased from Chimie Plus Laboratoires, France. The Ca/P ratio of the electrolyte is 1.67 similar as the stoichiometric ratio of hydroxyapatite (HA). The pH has been adjusted by sodium hydroxide addition. 0.2 $g.L^{-1}$ pluronic acid F127 was added or not as surfactant. A filtration was performed before out-of-phase sonoelectrodeposition with a 40 µm paper filter from Whatman, UK, in order to eliminate possible precipitates. The pH before electrodeposition were equal to 4.9, 5.1 or 9.3.

2.2. Synthesis methodology

Out of phase pulse sonoelectrodeposition requires a potentiostat to control the potential, and an ultrasonic generator to handle the pulses of the titanium working electrode. A thermostatic bath is used to increase the temperature of the electrolytic cell, while a cold air generator can cool the sonotrode to avoid damaging it. The assembly makes it possible to carry out pulsed sono-electrodeposition phase-shifted at temperatures of the order of 70 ° C (±1 ° C) while avoiding damage to the sonotrode, which has a limit of use of 80 °C (knowing that the ultrasound causes it to warm up).

The experimental setup schematically presented in fig. 2 includes:

- a computer part that manages via a remote control the control of ultrasound and potentiostat, a control software of the sonotrode NexTgen and Ec-Lab control software of the potentiostat SP-200 (Biologic).

- an electrochemical cell with three electrodes, incorporated in a thermostatic bath, comprising the titanium sonotrode which constitutes the working electrode, the auxiliary electrode in Platinum and the reference electrode Ag / AgCl / KCl inserted into a glass elongate. The electroactive part of the sonotrode was the 2 cm diameter planar circular surface at the bottom of the horn while the immersed cylindrical part into the electrolyte was covered by an isolating plastic jacket.

- a cooling system for the piezoelectric transducer of the sonotrode, consisting of a pure air generator that produces a pure air compressor which is then filtered.

After electrodeposition, the obtained CaP suspensions in the electrolyte were filtered under vacuum using a polycarbonate membrane with pores diameter of 100 nm, washed repeatedly with distilled water and dried at room temperature.

The out-of-phase pulsed sonoelectrodeposition synthesis was undergone at 70°C±1 ° C with the distribution of potential and ultrasound pulses with time presented in fig. 3. The applied potential during time t_{ON} (100 ms) was equal to -1.7 $V_{/AgAgCl}$. During this t_{ON} time, electrolysis takes place without ultrasound. Then an ultrasonic pulse during the t_{US} time (100 ms) with a resonance frequency of 19.5 kHz and a power of 200 W was used to remove electrodeposit from the surface of the TA6V horn acting as working electrode and to permit the expulsion of the particles into the electrolyte by cavitation. This ultrasonic pulse also allows the replenishment of the double layer by stirring the solution. At the end of the ultrasound time, a rest period without ultrasound and without polarisation was introduced to reduce acoustic streaming for a delay (t_{OFF}) equal to 100 ms. To synthesize enough powders for their characterization, the experiments were carried out for 3 times 300 s.

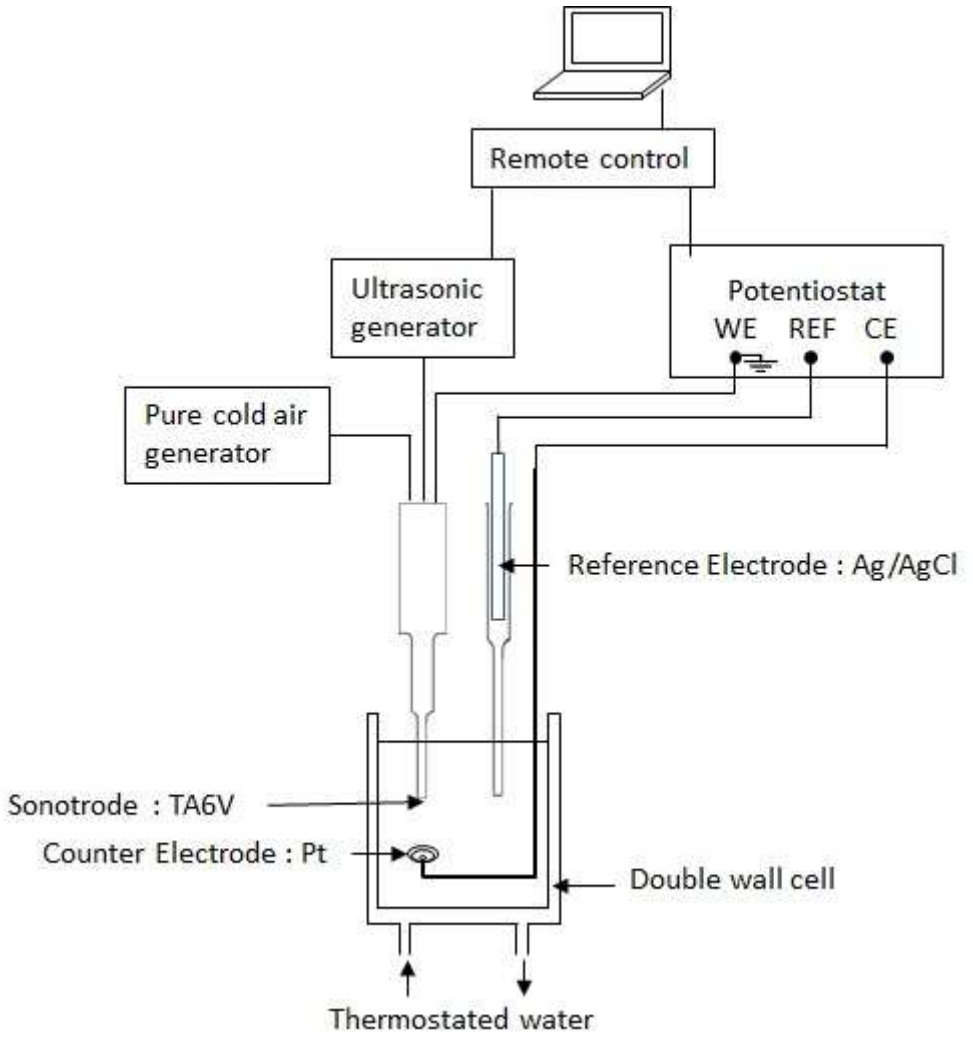

Fig. 2 – Experimental setup used for out of phase pulsed sonoelectrodeposition synthesis.

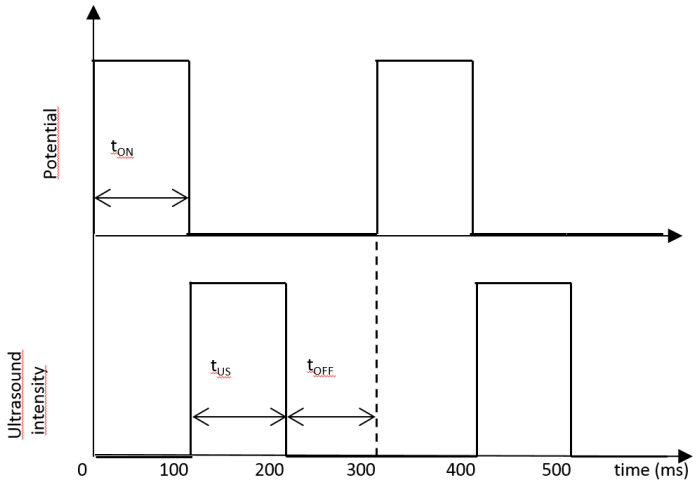

Fig. 3 – Distribution of the potential and the ultrasound pulses with time during the out-of-phase pulsed sonoelectrodeposition synthesis.

2.3. Characterization methods

2.3.1. Powder x-ray diffraction (PXRD)

The X-ray diffraction studies were done on the powders collected on the polycarbonate membranes. A D8 Advance (Bruker AXS GmbH, Karlsruhe, Germany) X-ray diffractometer equipped with a copper anticathode (λCuK_α= 0.154056 nm) was used in a Bragg-Brentano geometry for the PXRD experiments. The X-ray pattern data were acquired from 2θ = 4 to 80° with a step of 0.06° and exposure of 20 s at 40 kV and 40 mA. Phase's identifications were obtained using the Powder Diffraction Files (PDF) of the International Center for Diffraction Data (ICDD). The crystallite size has been estimated according to the Scherrer formula (Eq.(1):

$$\tau = 0.9\,\lambda/B \times \cos\theta \quad (1)$$

where τ is the crystallite size, λ is the wavenlength of monochromatic X-ray beam (λCuK_α= 0.154056 nm), B is the full width at half maximum (FWHM) of the peak of HA (002) reflection (rad), and θ is the diffraction angle (°) satisfying Bragg's law for the (002) plane.

2.3.2. Transmission electron microscopy (TEM) and Energy dispersive x-ray spectroscopy (EDX)

The structural morphology of the powders, captured on a Ni TEM grid, was observed by transmission electron microscopy using a JEM 1010 microscope from JEOL with an accelerating voltage of 100 kV and equipped with a digital CCD camera (ORIUS SC200W, GATAN). The Ca/P ratio was determined by energy-dispersive X-ray spectroscopy performed at 100 kV, using a Link ISIS spectrometer from Oxford Instruments, equipped with an ATW2 ultrathin window and associated to the TEM.

2.3.3. Fourier transform infrared spectroscopy (FTIR)

The functional groups of the powders were examined with a Fourier transform infrared (FT-IR) spectrometer Spectrum two (PerkinElmer).

3. Results and discussion

Fig.4 shows the potentiostatic cathodic i-t transients during the out-of-phase pulsed sonoelectrodeposition experiment with the electrolyte at pH = 4.9 with F127 Pluronic acid. In the first moment (Fig. 4.a) a rapid increase of current is observed followed by a decay in the following pulses, then, the current density stabilizes at an average constant value around -4.3 mA/cm^2 (Fig. 4.b) whilst regular oscillations are obtained during the experiment due to cavitation activity. The average current density of the other experiments is comprised between -3.8 mA/cm^2 and -8.2 mA/cm^2.

Due to the electrolysis some reactions occur in the electrolyte and at the cathode as follows:

$$(1)\ 2H_2O + 2e^- = H_2 + 2(OH^-)_{ads}$$
$$(2)\ O_2 + 2H_2O + 4e^- = 4(OH^-)$$
$$(3)\ HPO_4^{2-} + (OH^-)_{ads} = H_2O + PO_4^{3-}$$
$$(4)\ 10\,Ca^{2+} + 6\,PO_4^{3-} + 2OH^- = Ca_{10}(PO_4)_6(OH)_2\ (HA)$$
$$(5)\ (10\text{-}x)\,Ca^{2+} + (6\text{-}x)\,PO_4^{3-} + xHPO_4^- + (2\text{-}x)(OH^-)_{ads} = Ca_{10\text{-}x}(HPO_4)_x(PO_4)_{6\text{-}x}(OH)_{2\text{-}x}\ 0<x\leq 2\ (CDA)$$
$$(6)\ 8Ca^{2+} + 2HPO_4^{2-} + 4PO_4^{3-} + 5H_2O = 2Ca_4H(PO_4)_3 .5H_2O\ (OCP)$$

During the t_{ON} period the formation of hydroxyl ions resulting from water reduction allows the increase of pH near the sonotrode surface and hence promotes the precipitation of CaP (Eq. 4 and 5). The 100 ms electrochemical pulse is immediately followed by a 100 ms pulse of high intensity ultrasound (t_{US}) that removes the particles from the cathode surface and replenishes the double layer with cations by stirring the solution. A rest time (t_{OFF}) of 100 ms, without potential or ultrasonic vibrations, follows the two previous pulses, it is useful to restore the initial conditions close to the sonoelectrode surface. During this period, the ions-depleted region in the vicinity of electrode can be regenerated. As the power density of 200 W is sufficient, mechanical energy resulting from sonotrode causes a cavitation in the liquid, i.e. production and implosion of microbubbles which involves a mechanical erosion effect on the surface and expelses the precipitated particles far from the cathode surface avoiding their growth. Moreover, ultrasound permits also the acceleration of mass transport leading to enhance reaction rates. The stirring in the electrolytic bath changes the hydrodynamic conditions at the electrode/electrolyte interface with reduction of the diffusion layer thickness. The concentration gradient increases as well as the mass transport to the electrode.

The synthesized powders have been analyzed by XRD on the polycarbonate membranes used to separate them from the electrolyte. PXRD pattern are shown in Fig. 5. The peaks relative to the polycarbonate membrane are marked in black dashes. The influence of electrolyte pH on the calcium phosphate compounds is highlighted here, since the presence of octacalcium phosphate ($Ca_8(HPO_4)_2(PO_4)_4.5H_2O$; OCP) is mainly noticed in the pattern of the powder obtained at pH = 9.3 (Fig. 5d) with the peak at 2θ = 4.7°of the (100) reflection (ICDD 79-423). OCP is also present in the powder obtained at pH = 5.1 without F127. Hydroxyapatite ($Ca_{10}(PO_4)_6\,(OH)_2$; HA is identified in the pattern of powders at pH = 4.9 and 5.1 (Fig. 5a-c) with the characteristic

peaks at 2θ = 31.7° of the (211) reflection, 2θ = 32.2° of the (112) reflection and 2θ = 32.9° of the (300) reflection (ICDD 9-432), as shown for pH = 4.9 in the inset figure (Fig. 5) with Bragg's reflections in 2θ between 29°-35°. Those wide and in low intensity HA peaks are more in favour of a calcium-deficient hydroxyapatite or could testify the nanosize particles. Two others compounds DCPD ($CaHPO_4.2H_2O$; dicalcium phosphate dihydrate, brushite) and DCPA (CaHPO4 ; dicalcium phosphate anhydrous, monetite) have been characterized in these powders. DCPD is detected in pattern (a,b,c) and DCPA in pattern (a,d). Considering the (002) reflexion at 2θ = 25.88° the cristallite size of the powder synthesized from electrolyte at pH = 4.9 with F127 was estimated to 30 nm neglecting lattice strain.

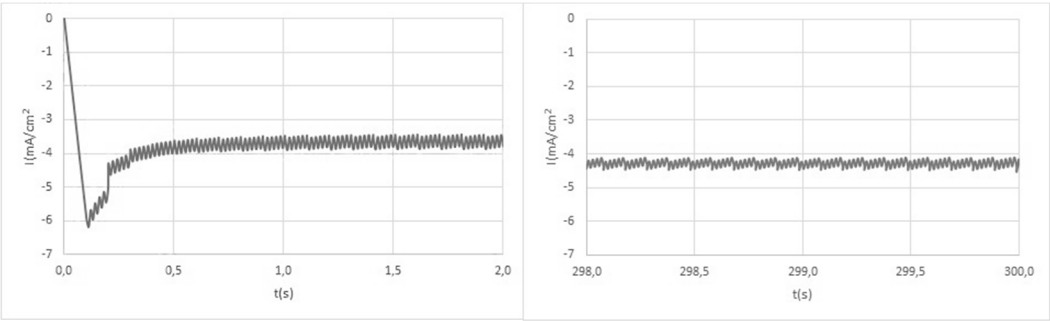

Fig. 4 – Current-time transients for deposition of CaP nanoparticles at -1.7V/AgAgCl during 300 s from electrolyte at pH = 4.9 with F127

(a) first 2 seconds and (b) ultimate 2 seconds

and (b) ultimate 2 seconds

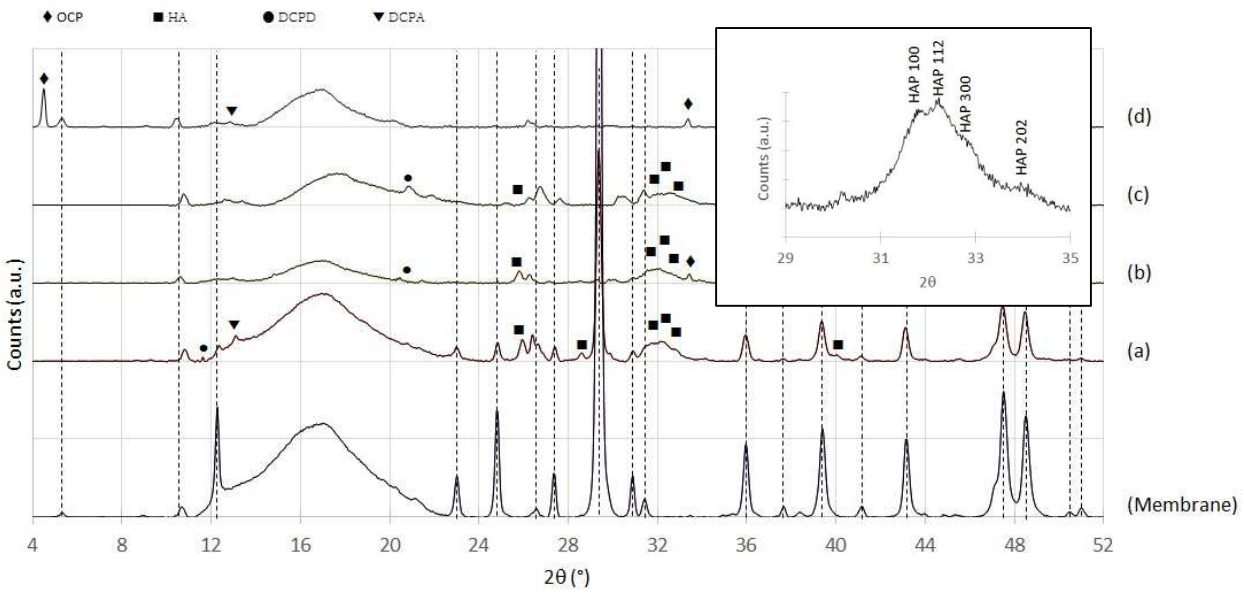

Fig. 5 – XRD pattern of the polycarbonate membrane and CaP NPs synthesized by out-of-phase pulsed sonoelectrochemical method at (a) pH = 4.9 with F127, (b) pH = 5.1 without F127, (c) pH = 5.1 with F127, (d) pH = 9.3 with F127, (e) polycarbonate membrane. Inset figure shows selected Bragg's reflections in 2θ between 29°-35° for CaP NPs synthesized by out-of-phase pulsed sonoelectrochemical method at pH = 4.9 with F127

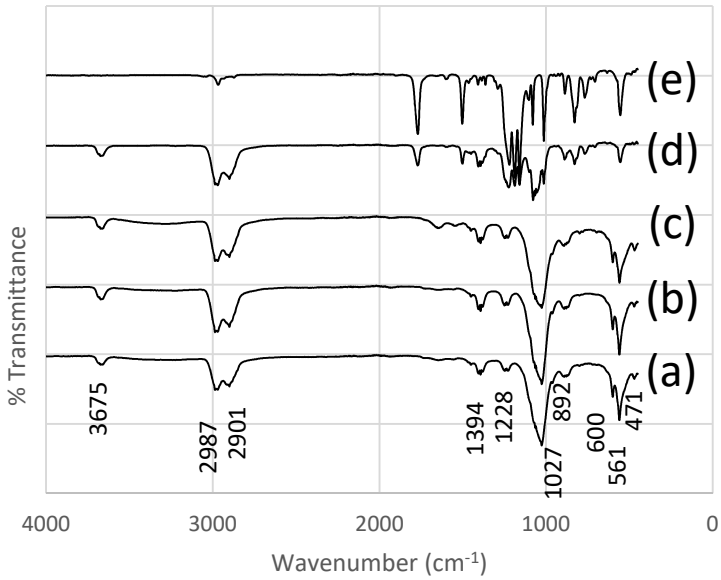

Fig. 6 – The FTIR spectra of the CaP NPs synthesized by out-of-phase pulsed sonoelectrochemical method at (a) pH = 4.9 with F127 (b) pH = 5.1 without F127, (c) pH 5.1 with F127, (d) pH 9.3 with F127, (e) polycarbonate membrane.

Table 1

Observed IR frequencies (in cm^{-1}) for CaP powders synthesized by out-of-phase pulsed sonoelectrochemical method at (a) pH = 4.9 with F127 (b) pH = 5.1 without F127, (c) pH 5.1 with F127, (d) pH 9.3 with F127.

(a)	(b)	(c)	(d)	Chemical groups	CaP phases (characteristic frequencies) references
471 sh	471 sh	469 sh		ν2 PO_4^{3-}	
561 vs	560 vs	560 vs	555 vs	ν4 PO_4^{3-}	Mixture (1027) [33]
600 sh	600 sh	600 sh		ν4 PO_4^{3-}	HA (602) [34]
			769 m		
			829 m	Out of plane (C H) def*	
892 m	892 m	892 m	890 m	ν3 CO_3 group	
960 w	960 w	960 w		ν1 PO_4^{3-}	
1027 vs	1027 vs	1027 vs	1028 vs	ν3c PO_4^{3-}	Mixture (1027) [33]
			1014 vs	Ns (O C O)*	
			1057 vs		OCP (1055-1058) [33]
1065 sh	1066 sh	1065 sh	1066 sh	ν3b PO_4^{3-}	
			1028 sh		OCP (1030) [34] / OCP (1023) [35]
1101 vw	1101 vw	1101 vw	1101 vw	ν3a PO_4^{3-}	
			1160 vs		
			1188 vs		
1228 m	1229 m	1229 m	1225 m		DCPD (1212) [35]
1250 m	1250 m	1250 m			
1394 m	1394 m	1394 m	1394 m		
1406 m	1406 m	1406 m	1407 m	CO_3 group	
			1502 vs	Ring ν (C-C)*	[36]
		1544 w			
		1645 w		H_2O bending	DCPD (1648) [33]
			1773 vs	ν (C=O)*	[36]
2901 s	2909 s	2901 s	2901 s		
2970	2970	2970 s	2970 s	Methyl ν_a(C-H)*	[36]
2987 s	2987 s	2987 s	2987 s		
3675 m	3675 m	3675 m	3675 m	O-H stretching	HA (3572) [33]

vw: very weak; w: weak; m: medium; s: strong; vs: very strong; sh: shoulder; *Polycarbonate.

The FTIR spectra of the CaP powders synthesized from electrolyte at pH = 4.9 with F127, pH = 5.1 without F127, pH = 5.1 with F127 and pH = 9.3 with F127 are shown in Fig.6 (a), (b), (c) and (d) respectively. CaP compounds have similar elementary constituents. The phosphate ions have modes of vibrations with signatures that are detected in all the IR spectra of CaP. Variations in the energies of phosphates could help to differentiate the different phosphocalcic phases due to their different structures. Furthermore, the existence of other ions or molecules for some of these phases, such as hydroxyl ions or water, can facilitate the identification of CaP phases. Absorption band at 471 cm^{-1} proves the presence of [PO4] groups, characteristic to tetrahedral apatite structure. The fundamental vibration modes of PO_4^{3-} at 560 cm^{-1} (asymmetric O-P-O bending mode), 600 cm^{-1} (O-H stretching vibration in HA) and 1027 cm^{-1} (asymmetric stretching vibration of P-O bond) were also shown on the FT-IR spectra for the powders obtained with electrolytes at pH 4.9 and 5.1 (Fig.6). Specific peaks in spectra (c) an (d) indicated by * correspond to polycarbonate membrane who was scraped with powders (Table 1).
The peak at 3675 cm^{-1} is due to the stretching mode of hydrogen bonded OH^- ions and can be attributed to the HA hydroxyl group, while the peak at 1027 cm^{-1} (v3 stretching mode of PO_4^{3-}) can be attributed to a mixture of HA, DCPD, DCPA and OCP [33]. Carbonate group was detected in every samples (890-892 cm^{-1} and 1406-1407 cm^{-1}) certainly due to environmental CO_2 absorption. Peaks at 1057 cm^{-1} and 1028 cm^{-1} in powder synthesized with electrolyte at pH = 9.3 can be attributed specifically to OCP [33-34] and confirm the major composition of this powder determined by PXRD analyses. The more basic pH of the electrolyte favors the precipitation of OCP. The bands in the range 2800-3100 indicate the presence of adsorbed water molecules on HA. The peak at 3675 cm^{-1} is a characteristic signature of HA in all the powders [33].

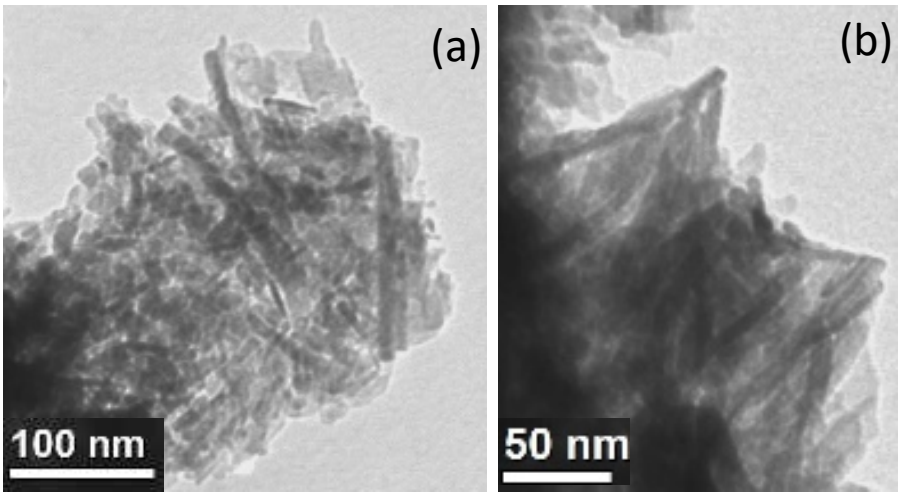

Fig. 7 – (a) and (b) TEM images of the CaP NPs synthesized by out-of-phase pulsed sonoelectrochemical method at pH = 4.9 with F127 Pluronic acid.

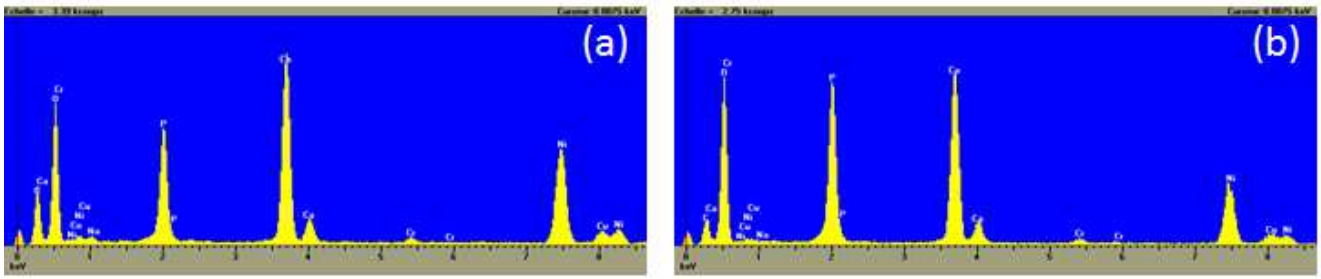

Fig. 8 – EDX spectra of the CaP NPs synthesized by out-of-phase pulsed sonoelectrochemical method at pH = 4.9 with F127 Pluronic acid. (a) CDHA with Ca/P = 1.54 ± 0.09, (b) DCPD or DCPA with Ca/P = 1.05 ± 0.13.

Analyses of a large quantity of the powder synthesized from the electrolyte at pH = 4.9 in the presence of pluronic acid F127 by EDX associated with Scanning electron microscopy give a Ca/P molar ratio of 1.59 indicating that the majority of this powder is composed of CDHA consistent with the wide peak on the powders diffraction pattern (Fig 5.a).

TEM examination of this powder (Fig.7a) reveals polycristalline nanorods with an average diameter of 6 nm and length up to 180 nm.These dimensions correspond to an aspect ratio l/d (length/diameter) equal to 30. This aspect ratio is similar to that obtained for nanowires synthesized in polycarbonate membranes with pore diameters of 200 nm by the template method [37] on a scale 45 times smaller. These nanowires electrodeposited in membranes had a

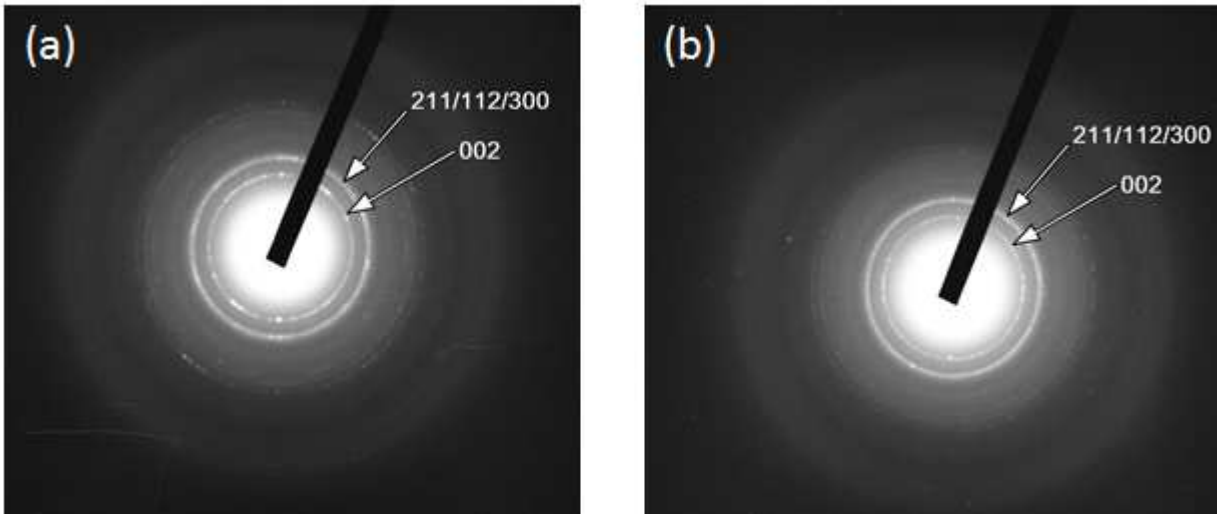

Fig. 9 – Indexed Selected Area Electron Diffraction patterns of the CaP NPs synthesized by out-of-phase pulsed sonoelectrochemical method at pH = 4.9 (a) and at pH = 5.1 (b) with F127 Pluronic acid.

diameter of 260 nm for a length of 8 µm and therefore an aspect ratio of 31.

Energy dispersive X-ray analyses associated with TEM reveal the presence of calcium deficient hydroxyapatite (CDHA) with Ca/P = 1.54 ± 0.09 and DCPD or DCPA with Ca/P = 1.05 ± 0.13 in the powder obtained from electrolyte at pH = 4.9 with F127.
Selected Area Electron Diffraction patterns were performed with the TEM at 100KV (Figure 9). For all samples, two main diffraction rings at 0.28 nm and 0.34 nm were observed corresponding to the diffraction reflections by the 002 and 211/112/300 crystallographic planes of an apatitic crystal structure.

This study confirms the interests of the sonoelectrodeposition method reported by others authors [38-41]: more uniform, smaller and purer crystals with minimal agglomeration. A narrow size distribution and a small size of particles are favored by the ultrasounds application. In agreement with Uskokovic, we can confirm that such a synthesis method favoring a fast crystallization (such as in this study with the ultrasounds application just after a shortened deposition duration), favors nucleation instead of crystallization so making able to obtain small particles and monodispersity [42]. Comparatively other methods of synthesis have also allowed through the use of ultrasound to obtain smallest CaP nanoparticles [43].

4. Conclusion

Out-of-phase sonoelectrodeposition appears to be a useful tool to produce high aspect ratio CDHA nanorods. This process including cavitation phenomena could enhance the potential of these nanoparticles in numerous biomedicine applications. Different analyses (PXRD, FTIR, EDX) have been used to determine the nature of CaP phases. Change in the electrolyte pH modifies the calcium phosphate nanoparticles compositions and phases. From electrolyte with low pH (between 4.9 and 5.3) nanorods composition consisted mainly of calcium-deficient hydroxyapatite and at higher electrolyte pH (9.3) octacalcium phosphate was favored.
TEM analyzes highlighted that the nanorods are polycrystalline and have an aspect ratio up to 30, that is the same aspect ratio as NPs obtained by the template method on a scale 45 times smaller. The out-of-phase pulsed sonoelectrochemistry technic can be an alternative method, simple and cost effective to produce such nanoparticles.

Acknowledgements

This work was supported by the Fondation pour la Recherche Médicale, grant number DCM 20111223750 to Chopart.

REFERENCES

[1] S. Beaufils, A. L. Daltin, P. Millet, J. P. Chopart, Template-assisted cathodic electrodeposition of calcium phosphates nanowires, European Cells and Materials, 30, 4 (2015) 12.
[2] J.L. Xu, K A, Khor, J.J. Sui, J. H. Zhang, W. N. Chen, Protein expression profiles in osteoblasts in response to differentially shaped hydroxyapatite nanoparticles. Biomaterials. 30, 29 (2009) pp.5385-5391, 10.1016/j.biomaterials.2009.07.002
[3] Z. Xu, C. Liu, J. Wei, J. Sun, Effects of four types of hydroxyapatite nanoparticles with different nanocrystal morphologies and sizes on apoptosis in rat osteoblasts. J Appl Toxicol. 32, 6 (2012) pp.429-435, 10.1002/jat.1745
[4] Y. Hong, H. Fan, B. Li, B. Guo, M. Liu, X. Zhang, Fabrication, biological effects and medical applications of calcium phosphate nanoceramics. Mater Sci Eng R. 70 (2010) pp. 225–242, 10.1016/j.mser.2010.06.010
[5] S. V. Dorozhkin, Nanodimensional and nanocrystalline apatites and other calcium orthophosphates in biomedical engineering, biology and medicine. Materials. 2, 4 (2009) pp. 1975-2045, 10.3390/ma2041975
[6] K. Lin, C. Wu, J. Chang, Advances in synthesis of calcium phosphate crystals with controlled size and shape, Acta Biomaterialia 10 (2014), pp. 4071–4102, /10.1016/j.actbio.2014.06.017
[7] C. Qi, J. Lin, L. H. Fu, P. Huang, Calcium-based biomaterials for diagnosis, treatment, and theranostics, Chemical Society Reviews 47, 2, (2017) pp. 357-403, 10.1039/C6CS00746E
[8] M. Okada, T. Furuzono, Hydroxylapatite nanoparticles: fabrication methods and medical applications, Science and Technology of Advanced Materials,13:6 (2012), 064103, 10.1088/1468-6996/13/6/064103
[9] M. Sadat-Shojai, M. T. Khorasani, E. , Dinpanah-Khoshdargi, A., Jamshidi, Synthesis methods for nanosized hydroxyapatite with diverse structures, Acta Biomaterialia 9, 8 (2013) pp. 7591-7621, 10.1016/j.actbio.2013.04.012
[10] A. Magdziarz, J.C., Colmenares, In situ coupling of ultrasound to electro-and photo-deposition methods for materials synthesis, Molecules 22, 2 (2017) pp. 216, 10.3390/molecules22020216
[11] H. M. Han, S. V. Mikhalovsky, G. J., Phillips, A. W. Lloyd, Calcium phosphate sonoelectrodeposition on carbon fabrics and its effect on osteoblast cell viability in vitro. New Carbon Mater., 22, (2007) pp. 121–125, 10.1016/S1872-5805(07)60012-2
[12] J. Reisse, J. L., Deplancke, R. Winand, Device for the production of ultrafine powders, Patent WO 95/33871, 1994-06-03.
[13] I. Haas, S. Shanmugam, A. Gedanken, Pulsed Sonoelectrochemical Synthesis of Size-Controlled Copper Nanoparticles Stabilized by Poly(N-vinylpyrrolidone), J. Phys. Chem. B 110 (2006) pp. 16947-16952, 10.1021/jp064216k
[14] A. Aqil, H. Serwas, J. L. Delplancke, R. Jérôme, C. Jérôme, L., Canet, Preparation of stable suspensions of gold nanoparticles in water by sonoelectrochemistry, Ultrasonics Sonochemistry 15, 6 (2008) pp. 1055-1061, 10.1016/j.ultsonch.2008.04.004
[15] I. Haas, A. Gedanken, Synthesis of metallic magnesium nanoparticles by sonoelectrochemistry, Chemical Communications 15 (2008) 1795-1797, 10.1039/b717670h
[16] V. Zin, B.G. Pollet, M. Dabalà, Sonoelectrochemical (20 kHz) production of platinum nanoparticles from aqueous solutions, Electrochimica Acta 54 (2009) pp. 7201–7206, 10.1016/j.electacta.2009.07.001
[17] V. Mancier, J.L. Delplancke, J.L. Delwiche, M. J. Hubin-Franskin, C. Piquer, L. Rebbouh, F. Grandjean, Morphologic, magnetic, and Mössbauer spectral properties of Fe_{75} Co_{25} nanoparticles prepared by ultrasound-assisted electrochemistry, Journal of Magnetism and Magnetic Materials 281, 1 (2004) pp. 27-35, 10.1016/j.jmmm.2004.03.047
[18] M. Dabala, M., B. G. Pollet, B.G., Zin, V., Campadello, E., Mason, T.J., Sonoelectrochemical (20 kHz) production of Co65Fe35 alloy nanoparticles from Aotani solutions, J Appl Electrochem 38 (2008) pp. 395–402, 10.1007/s10800-007-9450-x
[19] V. Zin, M. Dabalà, Iron–chromium alloy nanoparticles produced by pulsed sonoelectrochemistry: Synthesis and characterization, Acta Materialia 58, 1 (2010) pp. 311-319, 10.1016/j.actamat.2009.09.009
[20] N.H. Luong, N.H. Hai, N.D. Phu, D.A. MacLaren, Co-Pt nanoparticles encapsulated in carbon cages prepared by sonoelectrodeposition, Nanotechnology 22, 28 (2011) 285603, 10.1088/0957-4484/22/28/285603
[21] N. Hoang Nam, N. Thi Thanh Van, N. Dang Phu, T. Thi Hong, N. Hoang Hai, N. H. Luong, Magnetic properties of FePt nanoparticles prepared by sonoelectrodeposition, Journal of Nanomaterials (2012) 801240, 10.1155/2012/801240
[22] N.H. Luong, T.T. Trung, T. P. Loan, L.M. Kien, T.T. Hong, N.H. Nam, Magnetic Properties of FePd Nanoparticles Prepared by Sonoelectrodeposition, Journal of Electronic Materials 45, 8 (2016) pp. 4309-4313, 10.1007/s11664-016-4565-7
[23] V. Mancier, A. L. Daltin, D. Leclercq, Synthesis and characterization of copper oxide (I) nanoparticles produced by pulsed sonoelectrochemistry, Ultrasonics Sonochemistry 15, 3 (2008) pp. 157-163, 10.1016/j.ultsonch.2007.02.007
[24] Q. Shen, L. Jiang, J. Miao, W. Hou, J. J. Zhu, Sonoelectrochemical synthesis of CdSe nanotubes, Chemical Communications 14 (2008) pp. 1683-1685, 10.1039/b718022e
[25] R. Ganesan, S. Shanmugam, A. Gedanken, Pulsed sonoelectrochemical synthesis of polyaniline nanoparticles and their capacitance properties. Synth. Met. 158 (2008) pp. 848–853, 10.1016/j.synthmet.2008.06.001
[26] V. Mancier, C. Rousse-Bertrand, J. Dille, J. Michel, P. Fricoteaux, Sono and electrochemical synthesis and characterization of copper core-silver shell nanoparticles, Ultrasonics Sonochemistry 17, 4 (2010) pp. 690-696, 10.1016/j.ultsonch.2009.12.009
[27] S. Levi, C. Rousse, V. Mancier, J. Michel, P. Fricoteaux, Synthesis and characterization of copper-silver core-shell nanowires obtained by electrodeposition followed by a galvanic replacement reaction in aqueous solution; Comparison with a galvanic replacement reaction in ionic media, Journal of Materials Research, 30, 22 (2015) pp. 3518-3527, 10.1557/jmr.2015.335
[28] C. Gardin, L. Ferroni, L. Favero, E. Stellini, D. Stomaci, S. Sivolella, E. Bressan, B. Zavan, Nanostructured Biomaterials for Tissue Engineered Bone Tissue Reconstruction. Int J Mol Sci. 13 (2012) pp.737–757, 10.3390/ijms13010737
[29] T.J. Webster, C. Ergun, R. H. Doremus, R. W. Siegel, R. Bizios, Enhanced osteoclast - like functions on nanophase ceramics. Biomaterials. 22(2001) pp. 1327-1333, 10.1016/s0142-9612(00)00285-4
[30] S. Gao, K. Sun, A. Li, H. Wang, Synthesis and characterization of hydroxyapatite nanofiber by chemical precipitation method using surfactants. Mater Res Bull. 48, 3 (2013) pp. 1003-1006, 10.1016/j.materresbull.2012.11.090
[31] D.O. Costa, S.J. Dixon, A.S. Rizkalla, One- and Three-Dimensional Growth of Hydroxyapatite Nanowires during Sol − Gel − Hydrothermal Synthesis. ACS Appl Mater Interfaces 4, 3 (2012) pp.1490-1499, 10.1021/am201735k
[32] Y. Zhao, Y. Zhang, Y. Zhao, Synthesis and Cellular Biocompatibility of Two Nanophase Hydroxyapatite with Different Ca/P Ratio. J nanoscience Nanotechnol, 11, 12 (2011) pp. 1-5, 10.1109/INEC.2010.5425187
[33] L. A. Karampas, C. G. Kontoyannis, Characterization of calcium phosphates mixtures, Vibrational Spectroscopy, 64 (2013) pp. 126-133, 10.1016/j.vibspec.2012.11.003
[34] W. Mróz, A. Bombalska, B. Budner, S. Burdyńska, M. Jedyński, A. Prokopiuk, E. Menaszek, A. Ścisłowska-Czarnecka, A. Niedzielska, K. Niedzielski, Comparative study of hydroxyapatite and octacalcium phosphate coatings deposited on metallic implants by PLD method, Applied Physics A: Materials Science and Processing 101, 4 (2010) pp. 713-716, 10.1007/s00339-010-5926-3
[35] I. V.Smirnov, J. V. Rau, M. Fosca, A. De Bonis, A.Latini, R.Teghil, V.I.Kalita, A.Yu.Fedotov, S.V.Gudkov, A.E.Baranchikov, V.S.Komlev, Structural modification of titanium surface by octacalcium phosphate via pulsed laser deposition and chemical treatment, Bioactive Materials 2, 2 (2017) pp. 101-107, 10.1016/j.bioactmat.2017.03.002

[36] R. G. Kraus, E. D. Emmons, J. S. Thompson, A. M. Covington, Infrared absorption spectroscopy of polycarbonate at high pressure, Journal of Polymer Science: Part B: Polymer Physics, Vol. 46, (2008) pp. 734–742, 10.1002/polb.21405
[37] S. Beaufils, Ph. D. University of Reims Champagne Ardenne, France (2018).
[38] J. Zhang, X. Zhan, X. Wen, B. Song, L. Ma, W. Peng, Effects of ultrasonic and dispersants on shape and composition of hydroxyapatite by reflux method. Inorg Mater 45 (2005) pp. 1362–1365, 10.1134/S0020168509120103
[39] A. Kuznetsov, A. Fomin, A. Veresov, V. Putlyaev, I. Fadeeva, S. Barinov, Hydroxyapatite of platelet morphology synthesized by ultrasonic precipitation from solution. Russ J Inorg Chem 53 (2008) pp.1–5, 10.1134/S0036023608010014
[40] Rouhani P, Taghavinia N, Rouhani S. Rapid growth of hydroxyapatite nanoparticles using ultrasonic irradiation. Ultrasonics Sonochemistry, 17, 5 (2010) pp. 853-856, 10.1016/j.ultsonch.2010.01.010
[41] M. A. Giardina, M.A. Fanovich, Synthesis of nanocrystalline hydroxyapatite from Ca(OH)2 and H3PO4 assisted by ultrasonic irradiation. Ceram Int 36 (2010) pp. 1961–1969, 10.1016/j.ceramint.2010.05.008
[42] V. Uskokovic, D. P. Uskokovic, Nanosized hydroxyapatite and other calcium phosphates: Chemistry of formation and application as drug and gene delivery agents. Biomed Mater Res Part B: Appl Biomater 96B (2011) pp. 152–191, 10.1002/jbm.b.31746
[43] A.S. Stanislavov, L.F. Sukhodub, L.B. Sukhodub, V.N. Kuznetsov, K.L. Bychkov, M.I. Kravchenko, Structural features of hydroxyapatite and carbonated apatite formed under the influence of ultrasound and microwave radiation and their effect on the bioactivity of the nanomaterials, Ultrasonics Sonochemistry, 42 (2018) pp. 84–96, 10.1016/j.ultsonch.2017.11.011